Benchmarking and Inter-Comparison of Sentinel-1 InSAR velocities and time series

Z.Sadeghi[a*], T.J. Wright[a], A.J.Hooper[a], C. Jordan[b], A. Novellino[b], L. Bateson[b], J.Biggs[c]

[a] COMET, School of Earth and Environment, University of Leeds, Leeds, UK

[b] British Geological Survey, Environmental Science Centre, Keyworth, Nottingham, UK

[c] School of Earth Sciences, University of Bristol, Bristol, UK

[*] Corresponding author, email:z.sadeghi@leeds.ac.uk

Key Points: InSAR, Comparison, Sentinel-1, Ground Motion

Abstract

Different InSAR algorithms and methods produce velocities and times series that are not identical, even using the same data for the same area. This inconsistency can cause confusion and be a barrier to uptake and widespread use of the data in the commercial sector. With the widespread availability of Sentinel-1 radar data and a suite of new algorithms in the commercial and academic sectors, it is timely to develop a method for comparison of different results. In this study, we focus on developing and testing an independent and robust methodology for assessment of different InSAR processing results. Our proposed method is adapted from the Terrafirma Process Validation project; we compare geocoded line-of-sight velocities and time series, density and coverage, as well as some qualitative metrics. We use Sentinel-1 data from an area in Glasgow (UK) processed using 4 different approaches. The main areas of ground motion are detected using all approaches, with all velocities consistent at 1.1 mm/yr (1 sigma). Sentinel-1 InSAR therefore provides comparable results that are independent of processing approaches. However, there are considerable differences in some aspects of the results, in particular in the density and coverage. We discuss the reasons for these differences and suggest a framework for validation that could be used in future national or pan-national ground motion services.

1 Introduction

Synthetic Aperture Radar Interferometry (InSAR) is an Earth Observation technique based on radar satellite imagery to measure surface deformation due to different phenomena with millimetre to centimetre level precision (Bamler and Hartl 1998; Gabriel et al. 1989; Hanssen 2001). In order to improve the performance in extracting deformation signals from noisy InSAR data, different kinds of InSAR time-series approaches have been developed (Osmanoğlu et al. 2016; Pepe and Calo 2017). An innovative methodology known as Persistent Scatterer InSAR (PSI) was developed that exploited strong, stable scatterers that remain coherent for the entire time series of radar acquisitions (Ferretti et al. 2000, 2001). These techniques identify and isolate persistent scatterers (PS) that display coherent scattering behaviour over time to overcome temporal decorrelation, which restricts the use of conventional InSAR. By a combination of spatial and temporal filtering,

the contribution of atmospheric errors can also be reduced significantly. The original PS algorithms work where there are large number of strong scatterers (often man-made structures) with a deformation behaviour close to the assumed linear velocity model, although more sophisticated versions of the algorithm, capable of dealing with PS affected by non-linear motion, were soon presented. Later the Stanford Method for Persistent Scatterers (StaMPS) had been developed, with a focus on improving the number of measurement points in rural areas, and on providing an open source algorithm (Hooper et al. 2007). The major difference between StaMPS and the traditional PS approach is that StaMPS uses the spatial correlation of phase for identifying PS pixels. All PSI methods use a single-master stack of differential interferograms to process PS pixels (Hooper et al. 2012). For satellites, such as ERS-1/2 and Envisat, with a relatively large orbital tube, and hence a large range of perpendicular baselines in individual interferograms, only point scatterers remain coherent in a single master stack.

An alternative approach for extracting velocities and times series from InSAR uses information from Distributed Scatterers (DSs). These can contain coherent information when temporal and orbital baselines are relatively short/small but DS can be incoherent in interferograms with relatively long time intervals and large perpendicular baselines (different viewing geometries). The small baseline (SB) approach was developed to build time series by connecting small-baseline interferograms (Berardino et al. 2002; Schmidt and Bürgmann 2003). By combining PSI and SB approaches, hybrid approaches can increase measurement density (Hooper 2008; Lanari et al. 2004). There may still be highly useful interferometric measurements within the stack of SAR data that are excluded from a hybrid PS/SB analysis, particularly in rural areas where pixels may have intermittent coherence. A multi-interferogram method (Biggs et al. 2007) and ISBAS (Intermittent Small Baseline Subsets) method (Sowter et al. 2013), can exploit more of the coherent data to obtain average velocities. ISBAS and the multi-interferogram method are low-resolution approaches based on a minor modification of the SBAS method (Berardino et al. 2002) and can increase the number of measurement points, although without extracting any time series.

Recently, advanced methodologies for both PS and DS processing, notably the SqueeSAR algorithm, have been proposed to exploit all available information by forming all possible interferograms rather than small-baseline networks (Ferretti et al. 2011; Fornaro et al. 2015; Guarnieri and Tebaldini 2008). SqueeSAR selects neighbouring pixels with similar scattering mechanisms, known as statistically homogeneous pixels (SHP), and provides a proper synergistic analysis of PS and DS without the need for significant changes to the traditional PSI processing chain. It improves the density and quality of measurement points with respect to conventional PSI, over non-urban areas at the cost of a large increase in processing time. An alternative algorithm, RapidSAR (Rapid Time Series InSAR), was developed with capability of fast ingestion of new images and limited computational load (Spaans and Hooper 2016). This method identifies SHP pixels (named siblings) with a more computationally efficient algorithm than SqueeSAR. RapidSAR enables coherence in newly formed interferograms to be calculated quickly – the results

can be used in a modified SBAS approach to produce time series and velocities (Spaans and Hooper 2016).

Sentinel-1 is a two-satellite imaging radar constellation, providing global C-band imagery designed to supply the data needs of Europe's Copernicus programme. Sentinel-1A & -1B offer a six-day revisit cycle and unprecedented coverage of Europe, with 12-day imagery acquired globally. Sentinel-1 uses the Terrain Observation by Progressive Scan (TOPS) mode, sweeping the beam in the fight direction, and is designed primarily for InSAR applications (De Zan and Monti Guarnieri 2006). Raw data acquired by Sentinel-1 are freely available, addressing the limitation of cost and/or lack of data and providing research and commercial opportunities e.g. forming nationwide/international ground motion maps. All imagery is acquired within a narrow orbital tube, maximizing interferometric coherence. To exploit Sentinel-1 data, a European Ground Motion Service (EU-GMS) is under development, by the European Environment Agency (https://land.copernicus.eu/user-corner/technical-library/european-ground-motion-service), to provide consistent, regular, standardised, harmonised and reliable information on ground motion over Europe and across national borders, with millimetre accuracy. The ground motion results will be derived from time series analyses of Sentinel-1 data, most likely using different PS and DS InSAR approaches. Several Copernicus Participating States (e.g. Germany, Italy, Norway, Spain, Denmark, and France) have already or are in the process of implementing national ground motion services. These services will benefit from EU-GMS by standardising national service components and encouraging the use of deformation data by both public and commercial users. To make the outputs useful for operational applications, quality assessment of ground motion maps is a fundamental priority, and an important aspect of quality assessment is data consistency, particularly at borders or boundaries between different providers. A variety of InSAR time series have been developed by companies, universities and research establishments and their products can be dissimilar in terms of different metrics. The nationwide/international ground motion map will be likely processed by multiple suppliers, therefore there is a need to assess and ensure consistency of InSAR results.

Our main goal in this research is to develop and test a fair and robust methodology to assess the similarities and differences between results from different InSAR processing chains, and to recommend a validation strategy for any nationwide/international (e.g. UK/EU) ground motion map. We review the history of InSAR comparison approaches in Section 2. In Section 3, we describe an approach we have developed. In section 4, we use the method to compare 4 processing algorithms for a test area in Glasgow. We present results in Section 5 and discuss the major differences and similarities between the InSAR results in Section 6, providing recommendations for future nationwide/international products and one approach for future validation activity. Finally, we summarise the main conclusions in Section 7.

2) Review of previous InSAR comparison/validation approaches

Several previous projects have compared and validated InSAR velocities and time series. Following the 2003 Fringe meeting, the European Space Agency (ESA) initiated a blind InSAR

validation project, named PSIC4 (Persistent Scatterer Interferometry Codes Cross Comparison and Certification for long term differential interferometry) in order to assess the performance of PSI for land deformation monitoring using Envisat and ERS images (Crosetto et al. 2007b; Raucoules et al. 2009). The main pre-processing steps of the methodology applied on the PSI dataset (Altamira Information (Crosetto et al. 2008a), DLR (German Space Agency) (Adam et al. 2005), Gamma Remote Sensing (Werner et al. 2003), IREA-CNR (Institute for Electromagnetic Sensing of the Environment National Research Council of Italy) (Berardino et al. 2002), TRE (Tele-Rilevamento Europa) (Ferretti et al. 2007), TUDelft (Delft University of Technology) (Kampes 2005), UPC (Catalonia Polytechnics University) (Mora et al. 2003), Vexcel (Van der Kooij et al. 2005)) were adjusting geolocation shifts and spatially referencing to the same reference area. The most relevant indicators used to compare the results were the average deformation rate and the density and distribution of the selected PS points. The PSIC4 test area was a coal mining area it the South of France, which was undergoing rapid subsidence and did not include stable features. The results showed that for the case under consideration, the main area of subsidence could not or, could only partly, be assessed by most of the InSAR teams due to the low density of PS in the area of interest. Moreover, the inter-comparison results displayed a standard deviation of deformation velocity discrepancies ranging between 0.6 to 1.9 mm/year. One of the most important conclusions of this project concerned the characteristics of the coal mining test site in which none of the conditions to measure deformation with millimetric accuracy by PSI was fully accomplished. The severe characteristics of the PSIC4 test site were i) abrupt nonlinear motion and ii) strong deformation magnitude according to the temporal capability of Envisat/ERS. It was concluded that the "strong deformation" characteristic cannot in principle be extended to the other types of SAR missions and alternative SAR missions with more frequent acquisition capability e.g. Sentinel-1 can develop the results of this study (Raucoules et al. 2009). PSIC4 used "blind conditions" with no *a priori* information about the deformation or the goal of the PSI analysis. In fact, the teams used a standard PSI approach instead of tailoring the processing to a specific objective, which could explain the lack of PS in the mining area. Considering the above points, PSIC4 demonstrated that, at that time, PSI performance was highly dependent on the application, and the limitations were real. A wider area inter-comparison, "Provence Inter-Comparison", was later presented using the same data as PSIC4 but covering a larger area, including both deforming and stable areas (Crosetto et al. 2007a). A key difference in the Provence Inter-comparison study, compared to PSIC4, was comparing the dataset in the radar coordinate systems, to avoid validation issues associated with geocoding errors. When comparing the results of the two projects, there is an increase in performance in the case of the Provence inter-comparison for both the deformation velocity maps and the time series (Crosetto et al. 2007a). The Provence inter-comparison is largely based on data outside the mining area, which were simply not analysed in PSIC4 as these were not the areas specified as being of interest. It should be mentioned that the results of the two projects are not inconsistent and in most cases the results are rather similar.

The Terrafirma project (Capes et al. 2009), part of the EU/ESA Global Monitoring for Environment and Security (GMES) programme, the precursor to Copernicus, established a PSI

process validation approach, known as Terrafirma Validation Project, which built on the earlier studies. The Terrafirma validation project had two aims: results validation via comparison with ground truth levelling and inter-comparison of the results of different InSAR providers. The inter-comparison methodology compared four InSAR datasets from different providers (TRE, Altamira Information, Gamma Remote Sensing, and Fugro NPA) in radar coordinate systems to a reference processing result (GENESIS, DLR PSI processing), which was defined as the "truth" (Adam et al. 2009). Pre-processing steps included checking the global consistency of the datasets and the coregistration in radar space, referencing the data to the same reference in time and space dimension and removing potential tilts by de-trending. Velocities, time series, topographic corrections, detection capabilities and data densities were compared (Adam et al. 2007). This project produced a set of global statistics, which concerned large sets of PS pixels and provided information on the global inter-comparison behaviour of different metrics. The average standard deviation of the velocity differences and the mean standard deviation of the time series differences were 0.5-0.7 mm/yr and 1.5-5.6 mm, respectively. These values were used to derive error bars to indicate the quality of the estimate derived by PSI, which is key information for Terrafirma end users. Since deformation rates in the case studies in this project were moderately low, one should be careful in extending these statistics to areas involving higher deformation rates (Crosetto et al. 2008b). Moreover, the results showed remarkable differences in PS density between the providers, which resulted from the use of different criteria during PS selection (Crosetto et al. 2008c). As the Terrafirma PSI certification process was intended for local (20km×20km) PSI analysis of deformation, the Wide Area Processing (WAP) Terrafirma project later expanded this methodology to validate PSI processing over an area significantly greater (ERS scene of 100km×100km) than that considered in the initial Terrafirma PSI certification (Brcic et al. 2014). The results showed that the standard deviations of the deformation velocity differences for coherent pixels were below 1 mm/yr in most of the inter-comparison cases. This is one requirement of Terrafirma PSI certification. It also concluded that the most significant factors affecting compliance with this requirement are: (a) possible long wavelength trends affecting the interferograms (resulting from spurious atmospheric components and orbital fringes); (b) systematic phase components associated to the master scene used for the PS analysis, and (c) possible phase unwrapping errors, strongly dependent on the deformation signal and possible data gaps in the dataset.

Previous validation approaches have several limitations. Firstly, to be useful in real-world applications, InSAR data must be geocoded. By only comparing results from different methods/providers in the radar coordinate system means an important step of InSAR processing is excluded. Secondly, specifying a reference InSAR product as "truth", as done in the Terrafirma Validation Project, can also lead to an unfair comparison, as it excludes the possibility that the reference data set also has errors. Thirdly, validation projects to date have used data from Envisat and ERS; the improved spatial and temporal coverage of Sentinel-1 data, and its narrow orbital tube, open up several new opportunities for InSAR processing, which were not feasible previously.

Finally, previous approaches were only applied to validating PSI methods; a comparison method that can consider both PS and DS is now required.

Several recent studies have compared individual data sets or methods. A comparative study based on the results from DePSI (Delft PS-InSAR processing package) and StaMPS (Stanford Method for Persistent Scatterers), was applied using two datasets from ERS and Envisat and concluded that these methods are complementary in different aspects (Sousa et al. 2011). The time-series InSAR results generated using a PS method and a SBAS algorithm were compared quantitatively using ERS data and the calculated discrepancy was found to be consistent with those estimated by the PSIC4 study (Shanker et al. 2011). The capability of three InSAR time-series techniques, PSI, SBAS and SqueeSAR, for evaluating landslide deformation, was investigated using TerraSAR-X images (Mirzaee et al. 2017). The estimated average velocity maps and coherence maps produced by the methods were compared and it was concluded that SqueeSAR was more efficient for evaluating landslide kinematics in the rural case study. Performance of ISBAS and RapidSAR were compared using Sentinel-1 images to monitor shale-gas operations in Lancashire, outlined as part of an environmental monitoring research programme, and the results showed agreement between the approaches to estimate average annual velocity in the study area (Jordan et al. 2019).

With the Copernicus European Ground Motion Service now being commissioned, it is timely to formalise requirements for comparison of InSAR results. In this research, we present a methodology for inter-comparison of geocoded InSAR products using Sentinel-1 images. We test this methodology with the InSAR products resulted from different InSAR time series algorithms over a case study in which multiple InSAR datasets are available.

3 Methods

In this section, we introduce our new inter-comparison method. The outline of the proposed approach is shown in Figure 1. We base the approach on the Terrafirma Validation Project (Crosetto et al. 2008b), but tackle its limitations as follows: 1) As end-users require geocoded InSAR data, we compare all the datasets in geographic rather than radar coordinates. This allows us to consider any potential geocoding errors that can impact on the final product, especially areas with very local deforming. 2) Because no InSAR processing chain produces perfect, noise-free results, we avoid assuming that any reference InSAR processing is the "truth". 3) We define several polygons with different land cover types and stability. This allows us to assess how the agreement differs between InSAR data with changing the signal and/or type of features in the case study. 4) We do not limit the time series processing to PSI algorithms and are open to any other methodologies e.g. both PS and DS InSAR processing. 5) We work with Sentinel-1 imagery.

Our approach can be split into pre-processing and inter-comparison stages. These are described in more detail below.

3.1 Pre-processing

Before comparing data sets, some pre-processing steps are required:

(i) We assess the consistency of geocoded datasets from different InSAR methods. We convert the InSAR data to an identical geographic coordinate system. Any geocoding errors are critical when the deforming area is very small and should be noted. Adjustments can be made if necessary to ensure the data are comparable. This pre-processing step was applied in PSIC4 project. We assume that any translation of coordinates is constant for the whole data set; they can be assessed by overlaying the data on an accurate base map and considering some control points.

(ii) We select pairs of InSAR datasets for comparison, with each dataset processed using a different method. For the comparison to be valid, both data sets in a pair must use data from the same ascending or descending Sentinel-1 pass.

(iii) The time range of InSAR data making each comparison pair might be different. To ensure consistency as much as possible, we re-estimate the deformation velocity using a common time range for each comparison pair, by fitting linear velocities to the time series for each pixel using only data from the common time range.

(iv) We identify the common dates in the time series for each comparison pair and set the first common date as a reference time.

(v) We apply an identical low pass filter to each data set, in this case a triangular filter covering 5 epochs. This helps to remove the effect of random noise in a similar manner from both time series. Ideally, we work with unfiltered time series before applying this filter, but this may not always be possible.

(vi) We re-reference the deformation rate and deformation time series of all comparison pairs to an identical local reference area, which is outside the deforming areas and contains coherent pixels. Unlike the Terrafirma Validation Project, we do not have access to the coherence of selected points for all data sets. Therefore, we apply a noise analysis algorithm to identify high-quality pixels in the reference area (Hooper et al. 2007; Sadeghi et al. 2018). First, selected pixels are connected to form a network using Delaunay triangulation. Then, for each arc connecting two pixels, a weighted average phase is calculated from the entire time series, and removed from the original phase of the arc, which is then lowpass filtered in time. The resulting phase, with the weighted average phase added back in, provides an estimate for the smooth underlying signal. Phase noise is estimated by subtracting the smooth phase from the original phase of the arc. Finally, the phase noise of each measurement pixel is obtained from the phase noise of its corresponding arcs. The pixels with a noise level less than a threshold for all datasets are selected in the reference area.

(vii) The InSAR datasets forming the comparison pair are resampled to an identical geographic grid with 40 meters dimension in both easting and northing.

(viii) We define polygons covering areas with different scattering and deformation characteristics so that algorithms can be tested in different conditions. Therefore, the test site needs to i) have access to multiple InSAR dataset using Sentinel-1 images and

ii) cover areas with different characteristics. In the case of our test site in Glasgow, we define urban, rural and deforming polygons (see section 4 and Figure 2).

3.2 Inter-comparison of data sets

After applying the pre-processing steps, we compare InSAR results in terms of several metrics, including the estimated deformation rates, deformation time series, density and coverage as follows:

(i) We calculate the difference between deformation velocities for the common pixels of each pair and estimate Mean (μ_{dV}) and standard deviations (σ_{dV}) of the differences.

(ii) In order to extract statistics from the deformation time-series differences, (i) we compute the mean and standard deviation of the differences for each epoch of the time series at each common grid pixel; (ii) considering all common grid pixels of a given InSAR Provider (IP) pair, we calculate the mean of the parameters computed in the previous step, mean of mean of time-series differences $\mu\mu_{dD}$ and mean of standard deviation of time-series differences $\mu\sigma_{dD}$. The mean values show any potential bias between the estimated deformation velocities/time series of each pair. Standard deviation values provide information on how the deformation velocity/time series differences are distributed. We also calculate the correlation coefficient for estimated velocities (ρ_V) of all common grid pixels and estimated deformation time series (ρ_D) of each common grid pixel. This is a useful tool for measuring the degree of similarity of the deformation patterns of the analysed time series. In the ideal case, with identical deformation patterns, the correlation coefficient would be equal to one.

(iii) In order to compare the density and coverage of measurement pixels, we resample the InSAR data onto an identical 100 m by 100 m grid. The number of selected pixels in each cell gives the selected pixel density; we calculate the average density (*D*) for each of the polygons with different scattering/deformation characteristics. We also calculate the coverage of measurement pixels (*C*), which is determined by counting the percentage of grid pixels containing at least 1 selected pixel. We note that in order to make a fair comparison in terms of density and coverage, the noise analysis described above is applied before comparison and noisy pixels are removed using the same threshold for the phase noise standard deviation, in this case 1 rad.

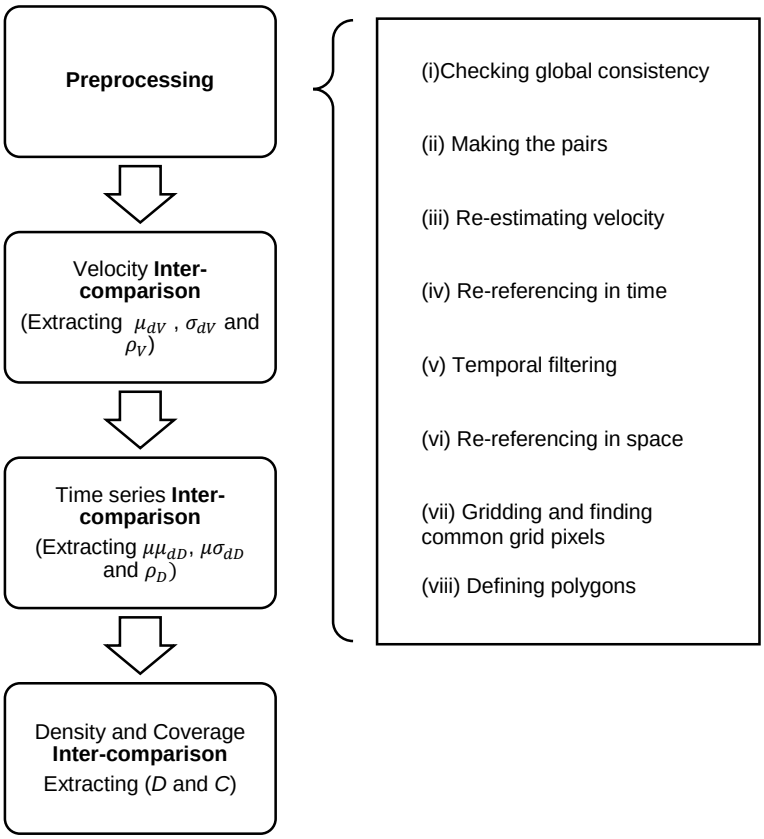

Figure.1) a flowchart showing our proposed inter-comparison methodology.

4 Data and Case Study

We use results from the Clyde Gateway of the Glasgow City Region to test our methods (Figure 2). This is an area of particular interest to the Natural Environment Research Council (NERC) as it is the British Geological Survey geothermal energy research field test site of the UKGEOS project (https://www.ukgeos.ac.uk/about/project-details). The Glasgow site will help characterise whether water from abandoned mine workings can be used to generate a sustainable and efficient source of energy. Changes in underground water levels, pressure and temperature caused by mine water for geothermal energy production activities can lead to surface subsidence/uplift (Heimlich et al. 2015). Therefore, monitoring is required to assess surface-level impacts of geothermal abstraction and re-injection research activities (Bateson and Novellino 2019). Although the area is largely urban, it also includes more rural areas, such as the Woodland park within the Cuningar loop.

We have access to multiple Sentinel-1 InSAR data products for this area, including data from SatSense processed using a modified RapidSAR algorithm (https://www.satsense.com) (Spaans and Hooper 2016), from TRE-ALTAMIRA processed using the SqueeSAR algorithm (https://site.tre-altamira.com) (Ferretti et al. 2011), and from GAMMA-IPTA processed using conventional PSI at BGS (https://www.gamma-rs.ch). Analysis and interpretation of some of the InSAR products can be found in (Bateson and Novellino 2019). We used these datasets as well as

our own analysis of Sentinel-1 using the conventional StaMPS algorithm which only processes PS pixels (Hooper et al. 2007) to test our InSAR inter-comparison activity. In all we have 5 data sets, 3 in ascending geometry and 2 in descending. Hereafter, we anonymise the IPs and label them A-D in no particular order. Table 1 compares the key characteristics of the data sets: the longest time span and the largest number of available images are related to A (Descending) and B (Descending) which used similar Sentinel-1 data sets, while C includes the shortest time range and smallest number of Sentinel-1 scenes. B and C used PSI algorithms which select only PS pixels and form single-master interferograms, but A and D took advantage of identifying both PS and DS pixels and made a multiple-master interferometric network. Apart from C, all of the InSAR data applied de-trending to remove any potential long-wavelength trend.

We define three polygons for the test region that broadly cover "deforming" (0.2 km^2), "urban" (0.9 km^2) and "rural" areas (1.2 km^2) (Figure 2). The area west of Cuningar Loop (deforming polygon) was a site developed for the Commonwealth Games Athletes Village and suffers from small 6 mm/yr rates of linear subsidence due to loading of the superficial deposits (Bateson and Novellino 2019).

Table.1) Key characteristics of the IP products: A-descending (Fig 3a), A-ascending (Fig 3b), B-descending (Fig 3c), C-ascending (Fig 3d), D-ascending (Fig 3e).

	Geometry	**Time range**	**Number of Scenes**	**Measurement Points**	**Interferogram Network**	**Trend removal**
A	Ascending (Fig 3c)	2015-05-23 2018-12-27	168	PS and DS	Multiple-Master	Yes
	Descending (Fig 3b)	2015-05-01 2019-02-27	175			
B	Descending (Fig 3d)	2015-05-01 2019-02-27	175	PS	Single-Master	Yes
C	Ascending (Fig 3e)	2015-08-15 2017-06-11	35	PS	Single-Master	No
D	Ascending (Fig 3f)	2015-03-12 2017-11-26	107	PS and DS	Multiple-Master	Yes

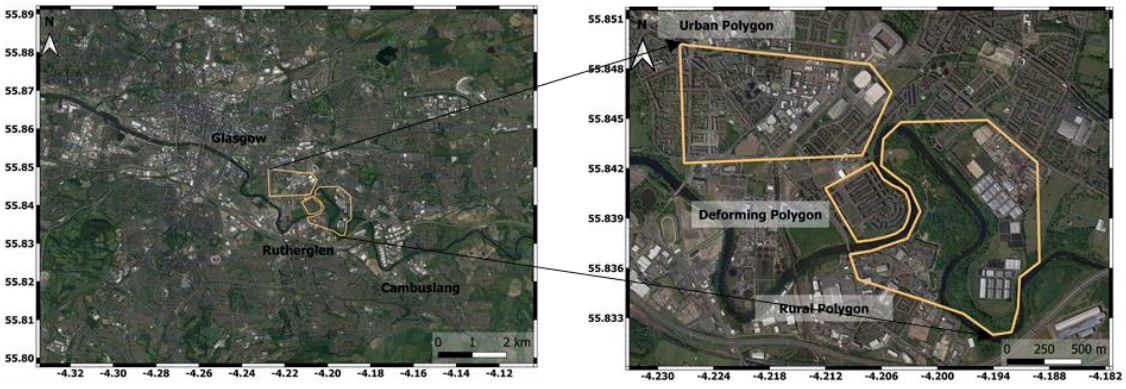

Figure.2) Location of our case study in Glasgow, the yellow outlined polygons are defined as areas including urban, rural and deforming features.

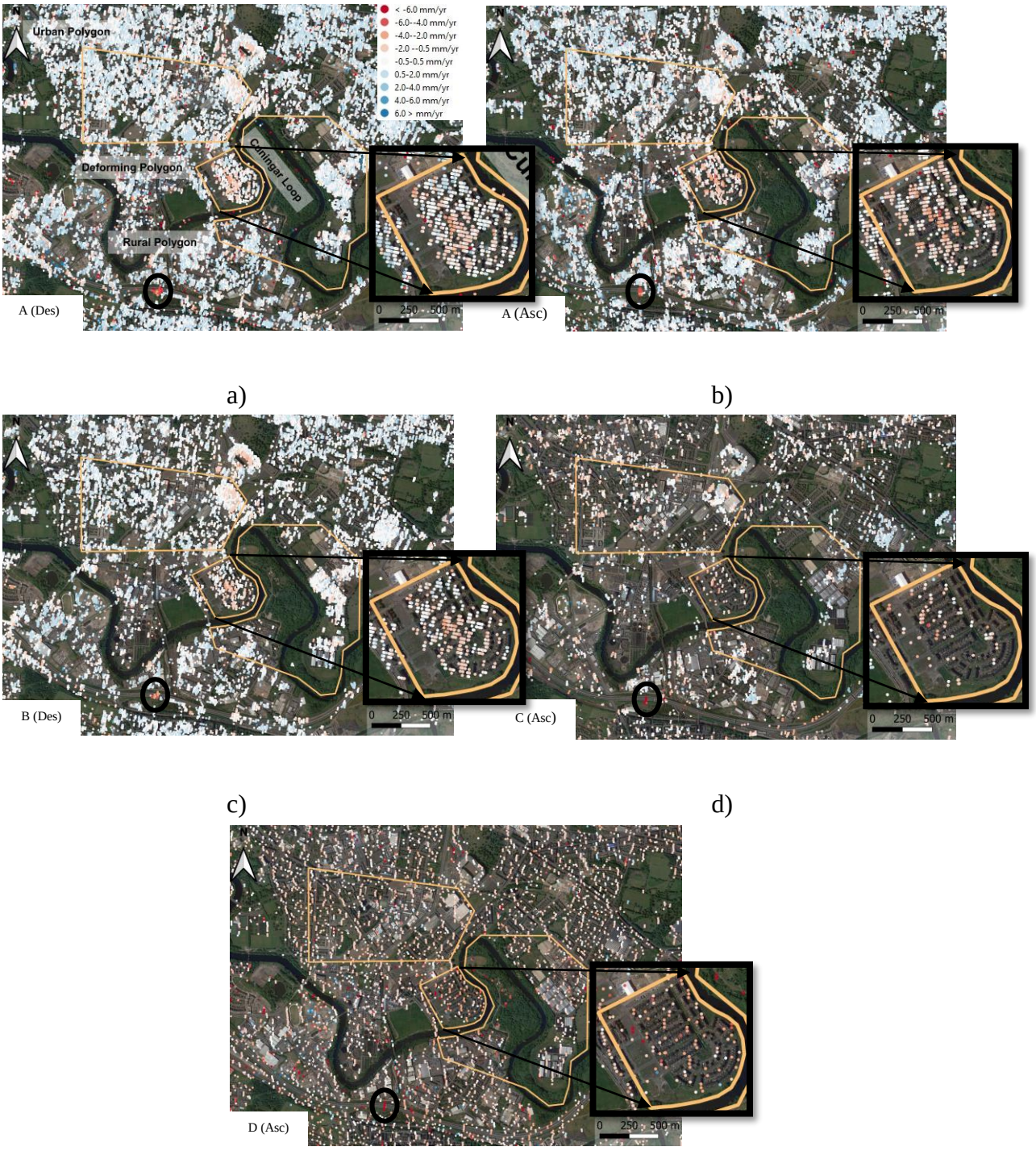

Figure.3) Estimated LOS deformation velocity in the case study by a) IP A using descending Sentinel-1 images, b) IP A using ascending Sentinel-1 images, c) IP B using descending Sentinel-1 images, d) IP C using ascending Sentinel-1 images and e) IP D using ascending Sentinel-1 images. The yellow outlined polygons are defined in a) as areas including urban, rural and deforming features. The black outlined ovals show a localised subsidence signal.

5 Results

In this section, we present the results of our inter-comparison methodology using the available datasets. Four InSAR comparison pairs can be made: A-B (descending), A-C (ascending), A-D (ascending) and C-D (ascending).

5.1 Inter-comparison of deformation velocity:

The velocity differences are calculated for the common grid pixels of each pair in the urban, rural and deforming polygons. The mean and standard deviation of deformation velocity differences and correlation coefficients of the estimated velocities are extracted and reported in Figure 4.

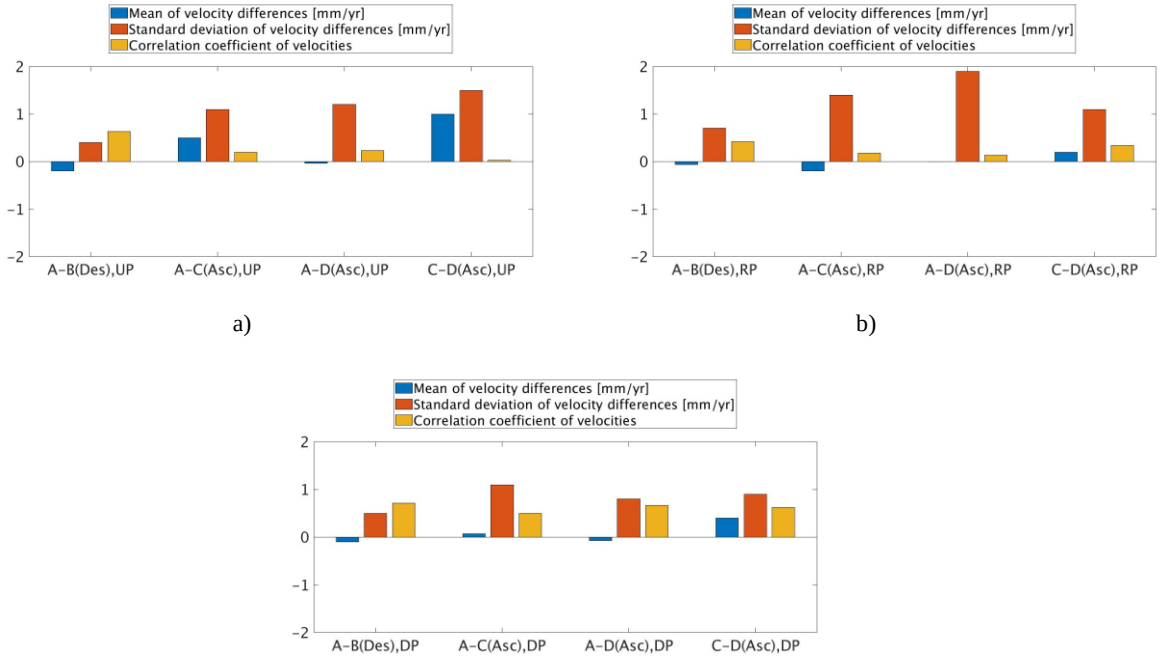

Figure.4) A bar chart showing the mean and standard deviation extracted from velocity differences and correlation coefficients between IP products, a) for urban polygon, b) for rural polygon and c) for deforming polygon. UP, RP and DP stand for Urban, Rural and Deforming Polygon.

The mean differences range between -0.002 mm/yr (A-D, rural polygon) and 1.0 mm/yr (C-D, urban polygon) and confirm that there are not any significant biases in estimated velocities. The estimated means associated with comparison pairs A-B and A-D are closer to zero than for A-C and C-D. The main reason for this is a long wavelength trend in IP C. The standard deviation related to A-B is well under 1 mm/yr and indicates a good global agreement. The standard deviations of the other IP pairs are all better than 2 mm/yr and the average of the standard deviation is highest in the rural polygon and lowest in deforming polygon for all pairs.

All InSAR comparison pairs show little correlation where there is little deformation (in the urban and rural polygons), but have higher correlation in the deforming polygon. Correlation coefficients are in the range 0.5 to 0.71 showing a good agreement between the different providers, where there is significant deformation. We illustrate the agreement by creating scatterplots of the estimated velocities in the deforming polygon (Figure 5). The correlation is clearest in the comparison between A and B, where both data sets have relatively high density, but a good correlation is seen in the deforming area for the other data sets, confirming that all algorithms are detecting deformation in this region.

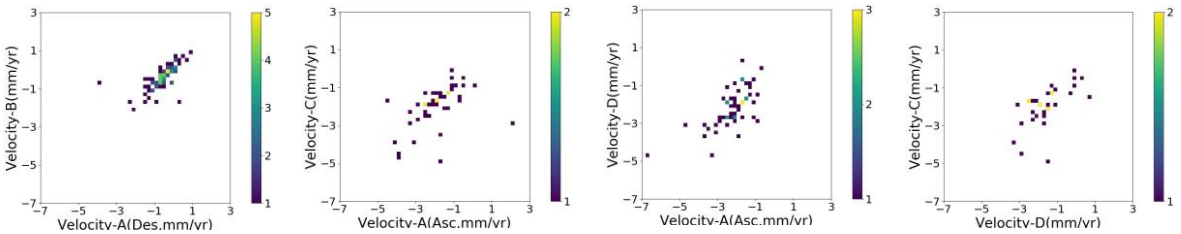

a) b) c) d)

Figure.5) Scatterplot of the estimated LOS velocities by a) A-B, b) A-C, c) A-D, d) C-D for deforming polygon. The color associated with each grid cell in the scatterplot shows the numbers of measurments points occupied.

5.2 Inter-comparison of deformation time-series:

As discussed in the Section 3, we calculate the differences between deformation time series in each comparison pair at each common grid pixels, and then extract mean and standard deviation of these differences at each pixel. Finally, the mean of the mean and mean of the standard deviation were estimated using all of the common grid pixels in each of the polygons (Figure 6).

The mean of mean values ($\mu\mu_{dD}$) is under ±2 mm for all pairs and indicate there are noticeable systematic effects between the time series of pairs. The mean of standard deviations ($\mu\sigma_{dD}$) ranges between 1 mm for the A-B pair and 2 mm for the A-D pair. Time series statistics associated with the A-D pair shows the poorest agreement with respect to the others for all polygons except urban polygon which mean of mean is slightly lower than A-B pair.

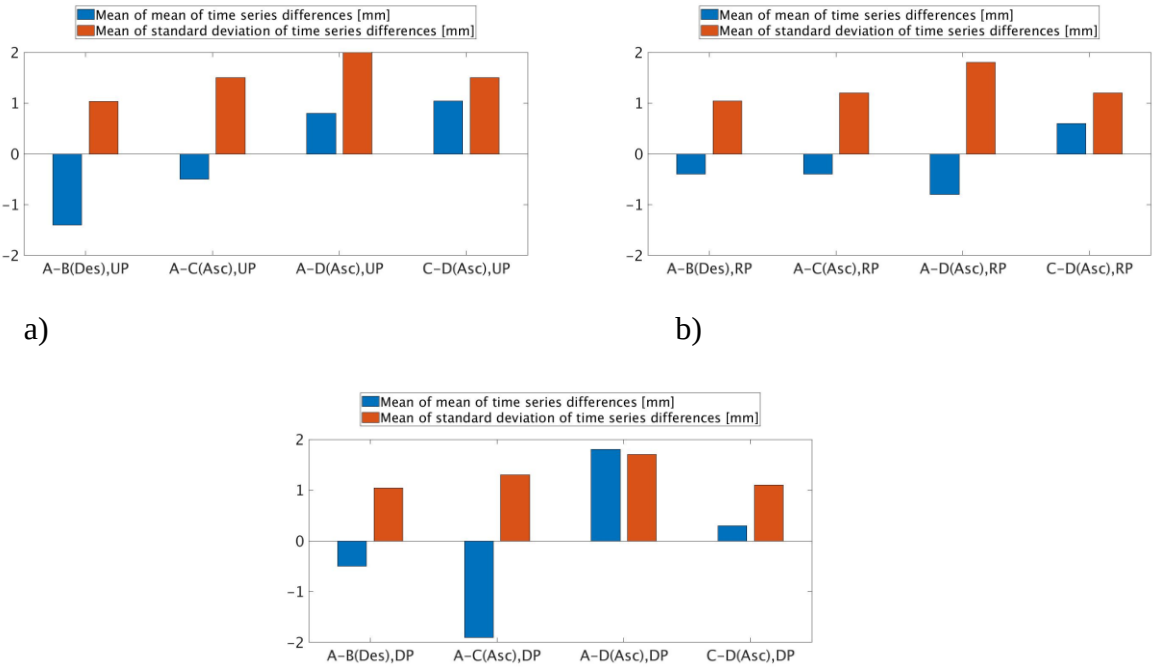

Figure.6) A bar chart showing the mean of mean and mean of standard deviation extracted from deformation time series differences of all common grid pixels between IP products a) for urban polygon, b) for rural polygon and c) for deforming polygon. UP, RP and DP stand for Urban, Rural and Deforming Polygon. The unit for the vertical axis is mm.

We also calculated the correlation coefficient for the estimated deformation time series of each common grid pixel and plotted the percentage of common grid pixels with a correlation coefficient above 0.7 in Figure 7. This figure confirms that the percentage above 0.7 is over 50% for all comparison pairs in the deforming polygon, which means more than half the common grid pixels in this polygon show a high level of similarity between the patterns of estimated deformation. Moreover, the most similar pattern of deformation for all polygons is related to the A-B pair.

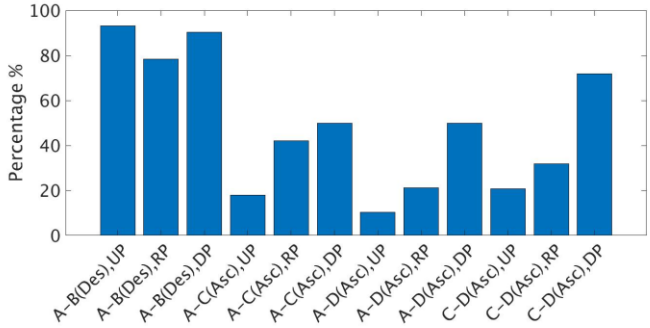

Figure.7) A bar chart showing the percentage of common grid pixels with correlation coefficient of deformation time series above 0.7. UP, RP and DP stand for Urban, Rural and Deforming Polygon.

We also compare the time series for one subsiding grid cell in the deforming polygon (Figure 8-a)) for all pairs. Figure 8-b) and 8-c) show the deformation time series plot and deformation time series scatterplot for A and B which used the same descending Sentinel-1 data sets. There is an excellent correlation coefficient between the deformation patterns estimated by the two IPs and any significant bias in the estimated deformation time series cannot be seen. The reference of the deformation time series is the first common date. The deformation time series with the original reference in time selected by the IPs are plotted in Figure 8-d) for A, C and D using descending Sentinel-1 images. Then the deformation time series for A-C, A-D and C-D (each comparison pair in ascending geometry) are plotted in the common temporal interval using the deformation of the first common date as a reference in time in Figure 8-e), 8-g) and 8-i), respectively. The corresponding scatterplots of the estimated deformation time series for A-C, A-D and C-D pair are shown in the Figure 8-f), 8-h) and 8-j), respectively and high agreements between the IPs in detecting the deforming signal can be seen.

5.3 Inter-comparison of density and coverage:

One major difference between the InSAR products is the density of pixels. We compare these for all IPs in Figure.9. All IPs provide the highest and lowest density in urban and rural areas, respectively. Moreover, density maps of different IPs are plotted in Figure.10. Both figures confirm that A is the most successful IP in terms of density of pixels for both ascending and descending geometry, and D identifies the lowest density.

We also compare the coverage for each InSAR comparison pair in Figure 11. The coverage of different IPs in the deforming polygons is very similar. Although D provided the lowest density for all polygons, it offers the highest coverage in rural and deforming polygons. Indeed, it was able to select pixels in some locations other IPs were not, e.g. inside the Cuningar loop in Figure 3.

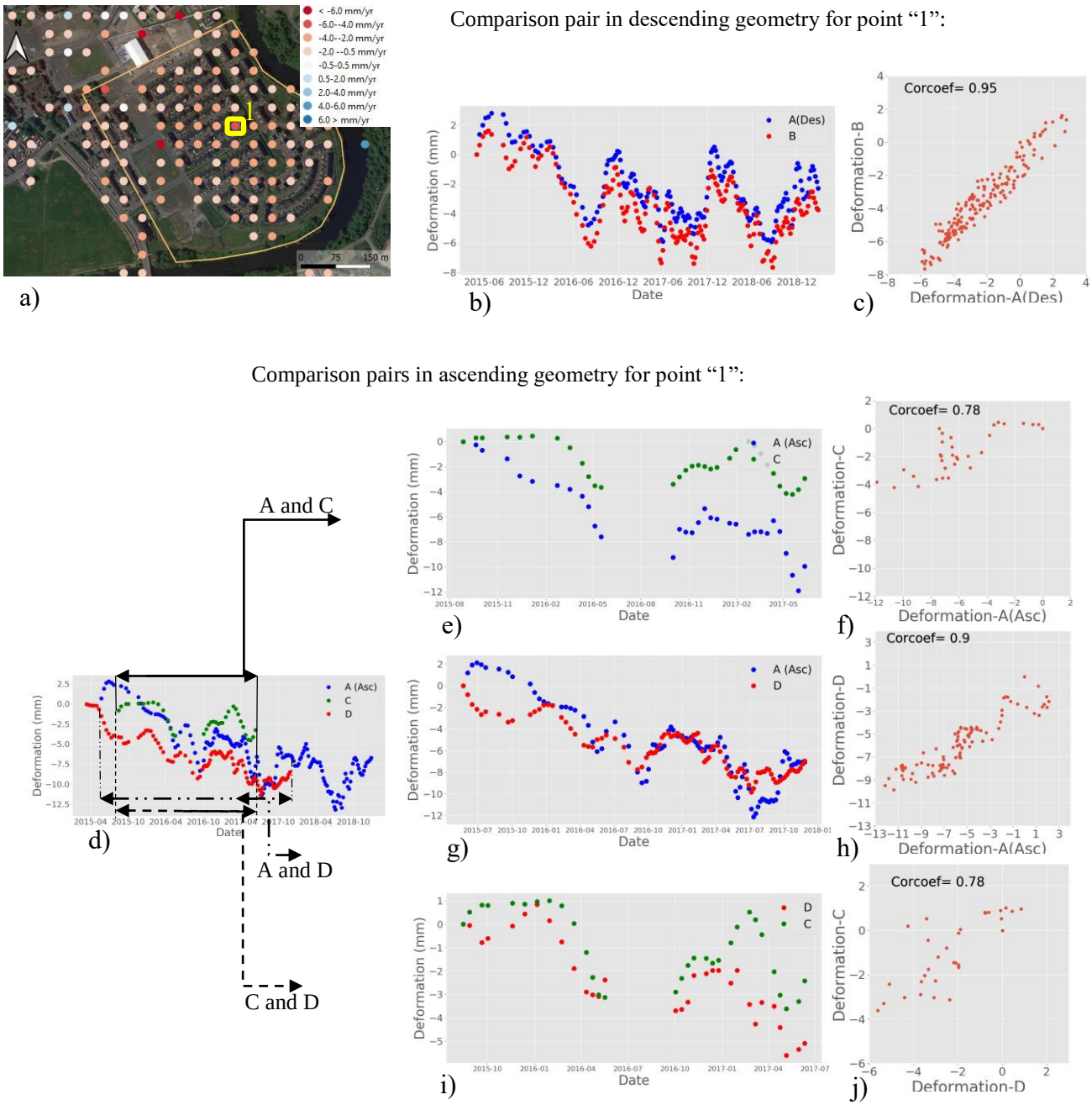

Figure.8) a) Estimated LOS velocity by A(Ascending) in the identical grid inside the deforming polygon, the estimated deformation time series and scatterplot of the deformation time series are plotted for the measurement grid pixel "1" using the InSAR data sets in b-j, b) deformation time series plot of A(Descending) and B (Descending) using the first common date as a reference in time, c) scatterplot of A(Descending) and B(Descending), d) deformation time series plot of A(Ascending), C(Ascending) and D(Ascending), the temporal reference of time series is the original reference selected by the IPs e) deformation time series plot of A(Ascending) and C(Ascending) in the common temporal interval using the first common date as a reference in time and f) scatterplot of A(Ascending) and C(Ascending) , g) deformation time series plot of A (Ascending) and D (Ascending) in the common temporal interval using the first common date as a reference in time and f) scatterplot of A (Ascending) and D (Ascending), i) deformation time series plot of C (Ascending) and D(Ascending) in the common temporal interval using the first common date as a reference in time and j) scatterplot of C (Ascending) and D (Ascending).

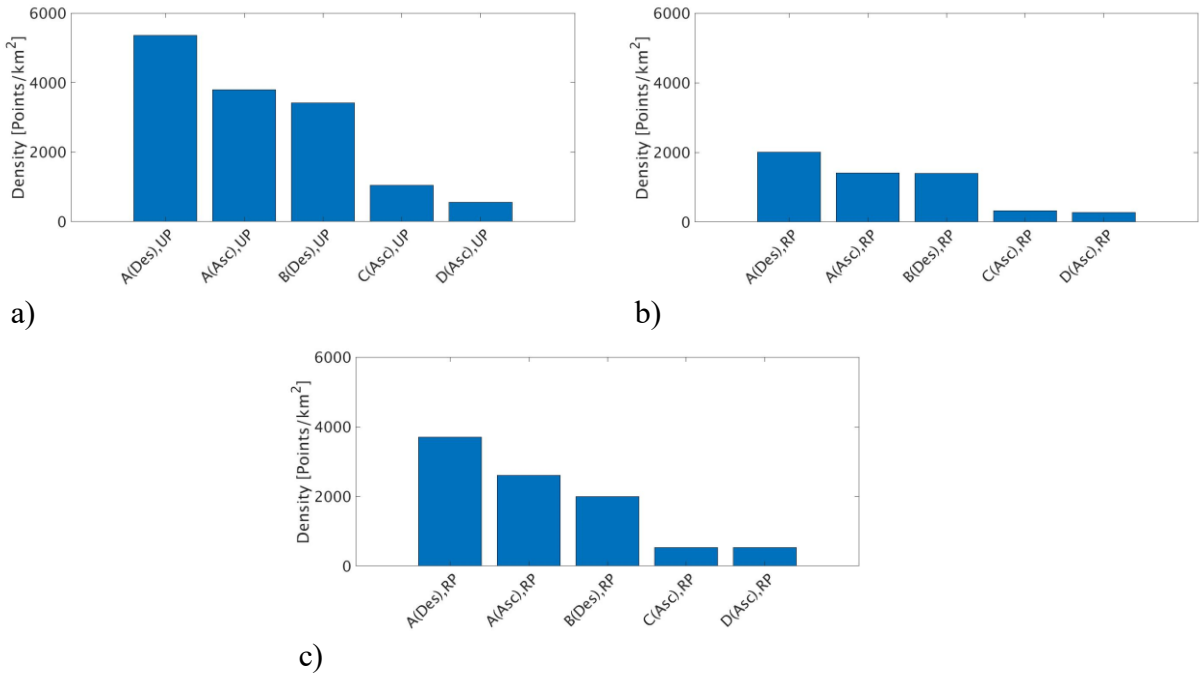

Figure.9) A bar chart showing the average density of measurement points by the IPs, for a) urban polygon, b) rural polygon and c) deforming polygon. UP, RP and DP stand for Urban, Rural and Deforming Polygon.

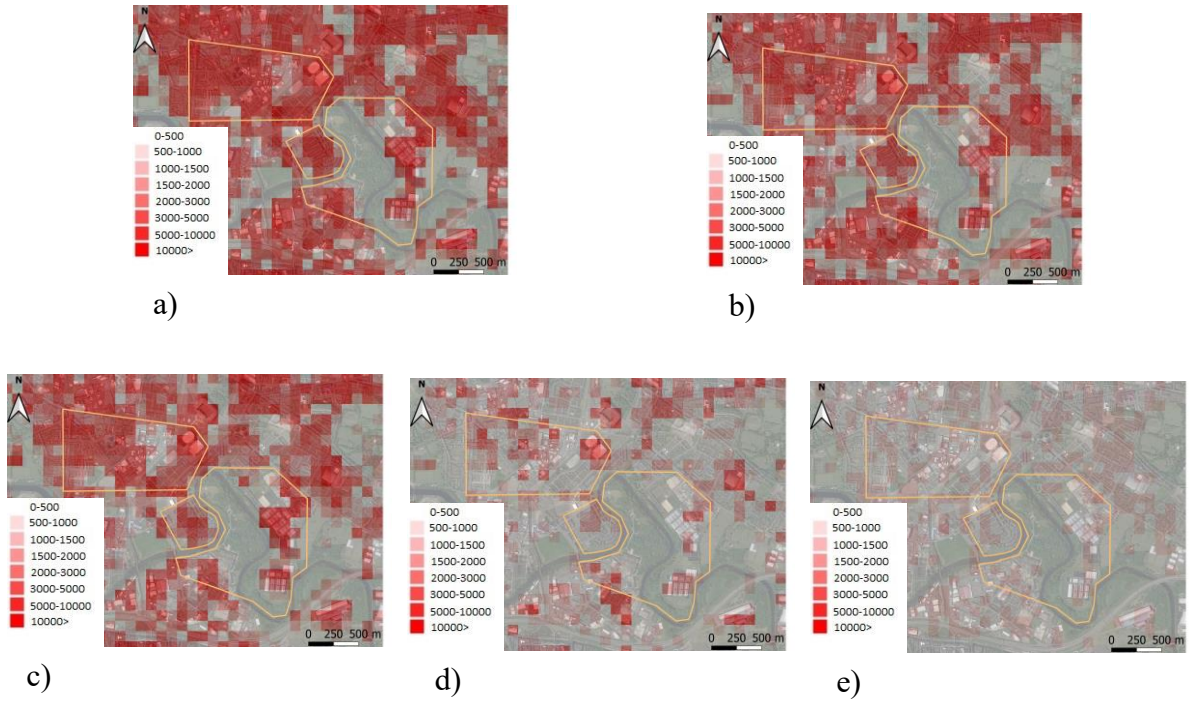

Figure.10) Number of measurement points in 1 km^2 by a) A (Descending), b) A (Ascending), c) B, d) C and e) D.

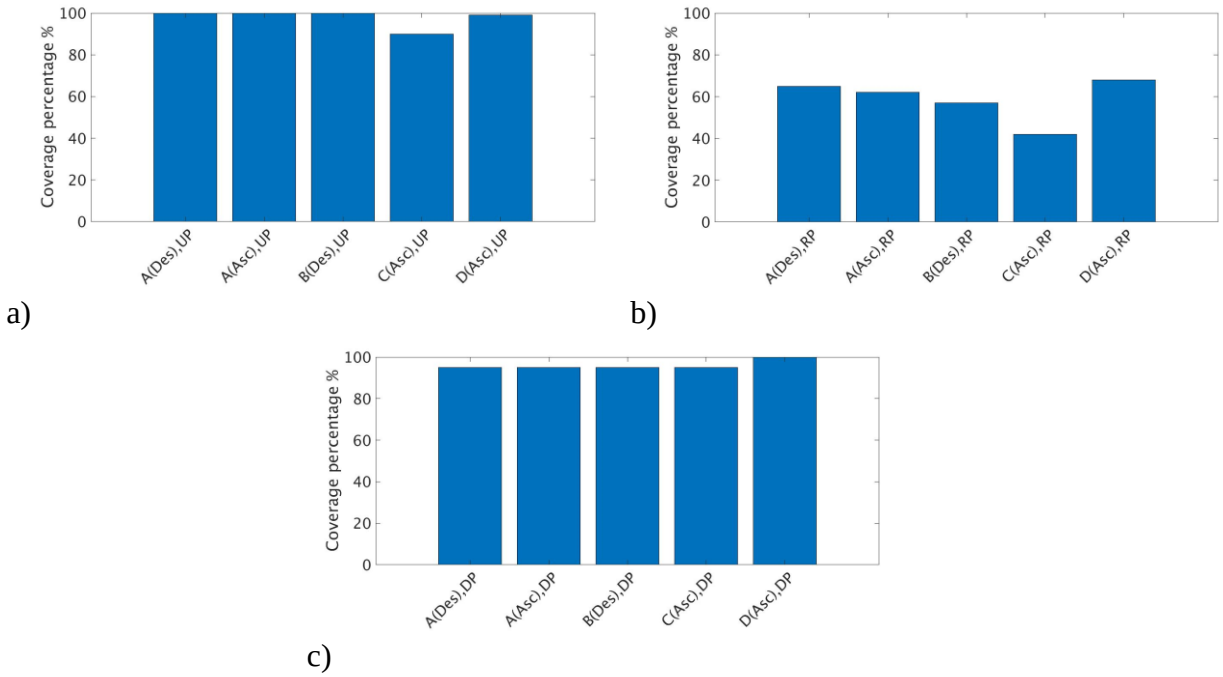

Figure.11) A bar chart showing the coverage of measurement points by the IPs, for a) urban polygon, b) rural polygon and c) deforming polygon. UP, RP and DP stand for Urban, Rural and Deforming Polygon.

6 Discussion and Recommendations

In this section, we discuss the major similarities and differences between InSAR results and discuss why they are different. We recommend some requirements for a national/international ground motion map. The major similarity between all the InSAR data sets is that they all detect similar deformation signals in the deforming polygon. Moreover, all of the methods provide a good density of observations in the urban polygon, as bright scatterers are selected appropriately by all the methods. In addition to the motion in the deformation polygon, a number of other features of deformation are seen in all data sets. For example, all data providers show localised subsidence (up to 10 mm/yr) on the M74 motorway gantry highlighted with black outlined ovals in Figure 3, which is likely related to instability in the embankment supporting the motorway at this location (Bateson and Novellino 2019).

However, the results are not completely identical. One of the most striking differences between different InSAR methods is density and coverage of selected pixels. The ability to recover measurements at a high pixel density and with wide coverage is one of the most important requirements for monitoring many different sources of deformation. This can be critical where the deforming signal is very local and occurs in non-urban areas that lack man-made structures. The main reason for the difference in point density is the different methodologies used for processing and the criteria that are used for selecting the pixels (Table 1 and Figure 9). In general, those methods that take advantage of both PS and DS, and benefit from making all possible interferograms (e.g. A and D) are more successful at extracting the maximum information (density

and/or coverage) from the SAR stack. However, due to the short baseline of the Sentinel-1 interferograms, some DS pixels can remain coherent in a single-master interferogram network and would be identified as PS pixels in PSI processing methods such as StaMPS, where phase correlation rather than amplitude is used to identify PS (Hooper et al. 2007). Fully connected networks including interferograms with long temporal baselines suffer from fewer selected pixels compared to the networks with only short baselines. Therefore, in addition to considering both PS and DS, other factors such as the temporal sampling of signal, the configuration of the interferometric network, whether oversampling of the original images is applied, and the specific thresholds imposed on signal-to-noise ratio (SNR) for pixel selection, can all have a major impact on the density of measurements.

Using a same level of SNR threshold by IPs for pixel identification can help to increase the consistency of the measurement points density. The sampling rate is such that the single-look pixel spacing is finer than the resolution, and some scatterers can therefore result in more than one PS pixel. In this case the IP should ensure that any extraneous PSs from a single scatterer are pruned. It should also be noted that time series methods selecting DS pixels can introduce data redundancy when spatial filtering is used to select SHPs. Therefore, given a homogeneous area, the selected points may show identical scattering behaviours. In this case, IPs should provide end-users the resolution of the DS pixels and inform them that those measurements do not correspond to that specific point. Techniques that use pixels with intermittent coherence (Biggs et al. 2007; Cigna and Sowter 2017; Sowter et al. 2013) can be more successful in terms of spatial coverage and density, particularly in non-urban areas; however, these methods tend to use a high multi-looking factor to improve coherence, and hence the density of observations is often lower.

Although high density of measurement points is a desired outcome for an InSAR product, striking a balance between the quality and density of selected pixels is challenging. A higher density can be obtained by not rejecting pixels with higher noise values. The interferometric processing strategy (e.g. the use of a single master or multiple master images) and the methodology of time series filtering/smoothing also have an impact on the level of noise in the final results. Decisions may need to be made on a case-by-case basis, depending on the application and the expected magnitude of the deformation signals. Although, it is clear that using the methodologies that not only provide high density, but also high quality, is one of the priorities for any national/international ground motion map.

There are some systematic effects in difference maps, which are mainly due to different approaches to dealing with long wavelength trends and atmospheric phase screens (APS). De-trending the products before inter-comparison would improve the data consistency, and it is be appropriate to de-trend data in future comparison activities.

Different geocoded coordinates for the common selected pixels is another discrepancy between the InSAR products. Overlaying InSAR data on an accurate base map or ortho-rectified aerial

photograph and/or using corner reflectors can be solutions for correcting the geocoding shifts. Although a linearly varying shift would probably provide more accurate geocoding corrections, in general, a constant shift is assumed for inter-comparison purposes (Raucoules et al. 2009). Geocoding error correction improves the agreement between different datasets significantly.

InSAR products are different in terms of some qualitative indicators. Spatial resolution is one of the most relevant metrics and ranges from the original high resolution sampling of Sentinel-1 (14.1 m and 2.3 m in azimuth and slant range direction, respectively) to lower resolutions that depend on the associated multi-look factors (e.g., 3 and 12 in azimuth and range direction, respectively). Some providers can provide both high and low resolutions to be used for different applications (e.g. rural and urban environments); this may be useful for national/international products.

We also note that ground motion maps are dynamic products, with velocities changing over time. Consequently, the frequency of update and latency period (time delay between acquisition and the update) should be defined by the IPs that deliver the product. An appropriate update and latency period should be defined as part of any commissioning process. Some applications, such as hazard monitoring, benefit from rapid updates.

Any future national or international ground motion service using Sentinel-1 InSAR will need to instigate a validation process to ensure data meet minimum standards and are consistent across borders. We propose that this is done in an open and transparent fashion. A single test region, or network of test sites for various applications, should be identified that includes a range of deformation and land cover types, and bidders should submit their analyses for this region as part of any commissioning process. The results should be open so that IPs benefit from understanding how their analyses differ from others and so that all can improve their offerings. One of our major challenges in this research, was that different Sentinel-1 images (ascending vs descending; different dates) were processed by the IPs, limiting our ability to conduct a fair comparison between all approaches. We suggest that a comparison exercise is repeated periodically and that in each case the time period and acquisition dates should be explicitly specified.

In our analysis, the IPs produced results over Glasgow to establish a baseline prior to the geothermal activity. The deforming areas in Glasgow were very local, and the scattering conditions in the deforming areas were not ideal. In addition, the “truth”, estimated through some independent measurement method, was unknown and therefore validation of the InSAR products using external measurements was impossible. Test sites should be carefully selected and should cover a range of different deformation types. Independent data should be collected, for example, from dense permanent networks of GNSS and levelling measurements. Corner reflectors may be useful for testing geolocation and for providing reliable measurement points, and it may be appropriate to process data from a very-high-resolution satellite system such as TerraSAR-X for additional validation of Sentinel-1 results.

7 Conclusions

In this research, we present an InSAR inter-comparison method, which 1) builds on the Terrafirma Validation Project and 2) addresses the limitations of proposed approaches up to now. We tested our method using 5 InSAR time series products including conventional PSI and advanced joint PS and DS InSAR, using Sentinel-1 images. We selected an inter-comparison site in Glasgow, for which we had access to multiple InSAR data, and defined three polygons covering urban, rural, and deforming features. It is clear from our results that different InSAR methods detect the same general deformation framework, but they are not identical in terms of different metrics. We propose different indicators, which are divided into quantitative metrics e.g. density and coverage of measurement points and qualitative metrics e.g. spatial resolution. Based on our comparison results, we suggest some recommendations, which might be useful for any future nationwide/international InSAR product and validation activities.

Acknowledgments

Benchmarking and Inter-Comparison of Sentinel-1 InSAR velocities and time series is part of Digital Environment project funded by NERC. COMET is the NERC Centre for the Observation and Modelling of Earthquakes, Volcanoes and Tectonics, a partnership between UK Universities and the British Geological Survey. Sentinel-1 data were obtained via the Copernicus Program of ESA. RapidSAR data were processed by SatSense Ltd. SqueeSAR data were processed by TRE-Altamira Ltd. GAMMA-IPTA data were processed by British Geological Survey (BGS). The authors are grateful to Dr. A. Ferretti for comments that improved the manuscript.

References

Adam, N., Kampes, B., & Eineder, M. (2005). Development of a scientific permanent scatterer system: Modifications for mixed ERS/ENVISAT time series. In, *Envisat & ERS Symposium, ESA*

Adam, N., Parizzi, A., Crosetto, M., & Bally, P. (2007). Terrafirma Report: Specification of Validation Approach Part 1: Process Validation.DLR-IMF-Remote Sensing Technology Institue,

Adam, N., Parizzi, A., Eineder, M., & Crosetto, M. (2009). Practical persistent scatterer processing validation in the course of the Terrafirma project. *Journal of Applied Geophysics, 69*, 1,59-65,doi:10.1016/j.jappgeo.2009.07.002.

Bamler, R., & Hartl, P. (1998). Synthetic aperture radar interferometry. *Inverse Problems, 14*, 4,R1-R54,doi:10.1088/0266-5611/14/4/001.

Bateson, L., & Novellino, A. (2019). Open Report: Glasgow Geothermal Energy Research Field Site - Ground motion survey report British Geological Survey, Available:http://nora.nerc.ac.uk/id/eprint/524555/1/OR18054.pdf.

Berardino, P., Fornaro, G., Lanari, R., & Sansosti, E. (2002). A new algorithm for surface deformation monitoring based on small baseline differential SAR interferograms. *IEEE Transactions on Geoscience and Remote Sensing, 40*, 11,2375-2383,doi:10.1109/TGRS.2002.803792.

Biggs, J., Wright, T., Lu, Z., & Parsons, B. (2007). Multi-interferogram method for measuring interseismic deformation: Denali Fault, Alaska. *Geophysical Journal International, 170*, 3,1165-1179,doi:10.1111/j.1365-246X.2007.03415.x.

Brcic, R., Parizzi, A., Rodriguez Gonzalez, F., & Duro, J. (2014). Technical Report: WP1500:WAP Comparison Plan. ESA GMES Service Element, ESRIN/Contract No. 4000109669/13/I-AM

Capes, R., Marsh, S., Bateson, L., Novali, F., & Cooksley, G. (2009). Terrafirma User Guide: A guide to the use and understanding of Persistent Scatterer Interferometry. ESA GMES Service Element, Available:https://core.ac.uk/download/pdf/385324.pdf.

Cigna, F., & Sowter, A. (2017). The relationship between intermittent coherence and precision of ISBAS InSAR ground motion velocities: ERS-1/2 case studies in the UK. *Remote Sensing of Environment, 202*,177-198,doi:https://doi.org/10.1016/j.rse.2017.05.016.

Crosetto, M., Agudo, M., Capes, R., & Marsh, S. (2007a). GMES Terrafirma: Validation of PSI for users: Results of the Provence inter-comparison. In, *Proceedings of the Envisat Symposium, ESA* (pp. 23-27)

Crosetto, M., Agudo, M., Raucoules, D., Bourgine, B., de Michele, M., Le Cozannet, G., Bremmer, C., Veldkamp, J., Tragheim, D., & Bateson, L. (2007b). Validation of Persistent Scatterers Interferometry over a mining test site: results of the PSIC4 project. In, *Envisat Symposium,ESA* (pp. 23-27)

Crosetto, M., Biescas, E., Duro, J., Closa, J., & Arnaud, A. (2008a). Generation of advanced ERS and Envisat interferometric SAR products using the stable point network technique. *Photogrammetric Engineering & Remote Sensing, 74*, 4,443-450

Crosetto, M., Monserrat, O., & Agudo, M. (2008b). Validation of existing processing chains in Terrafirma stage 2: Process analysis report-Part 2: IG inter-comparison. ESA GMES Service Element, Institut de Geomatica,

Crosetto, M., Monserrat, O., Bremmer, C., Hanssen, R., Capes, R., & Marsh, S. (2008c). Ground motion monitoring using SAR interferometry: Quality assessment. *European Geologist, 26*,12-15

De Zan, F., & Monti Guarnieri, A. (2006). TOPSAR: Terrain Observation by Progressive Scans. *IEEE Transactions on Geoscience and Remote Sensing, 44*, 9,2352-2360,doi:10.1109/TGRS.2006.873853.

Ferretti, A., Fumagalli, A., Novali, F., Prati, C., Rocca, F., & Rucci, A. (2011). A New Algorithm for Processing Interferometric Data-Stacks: SqueeSAR. *IEEE Transactions on Geoscience and Remote Sensing, 49*, 9,3460-3470,doi:10.1109/TGRS.2011.2124465.

Ferretti, A., Prati, C., & Rocca, F. (2000). Nonlinear subsidence rate estimation using permanent scatterers in differential SAR interferometry. *IEEE Transactions on Geoscience and Remote Sensing, 38*, 5,2202-2212,doi:10.1109/36.868878.

Ferretti, A., Prati, C., & Rocca, F. (2001). Permanent scatterers in SAR interferometry. *IEEE Transactions on Geoscience and Remote Sensing, 39*, 1,8-20,doi:10.1109/36.898661.

Ferretti, A., Savio, G., Barzaghi, R., Borghi, A., Musazzi, S., Novali, F., Prati, C., & Rocca, F. (2007). Submillimeter accuracy of InSAR time series: Experimental validation. *IEEE Transactions on Geoscience and Remote Sensing, 45*, 5,1142-1153,doi:10.1109/TGRS.2007.894440.

Fornaro, G., Verde, S., Reale, D., & Pauciullo, A. (2015). CAESAR: An Approach Based on Covariance Matrix Decomposition to Improve Multibaseline-Multitemporal Interferometric SAR Processing. *IEEE Transactions on Geoscience and Remote Sensing, 53*, 4,2050-2065,doi:10.1109/TGRS.2014.2352853.

Gabriel, A.K., Goldstein, R.M., & Zebker, H.A. (1989). Mapping small elevation changes over large areas: Differential radar interferometry. *Journal of Geophysical Research: Solid Earth, 94*, B7,9183-9191,doi:10.1029/JB094iB07p09183.

Guarnieri, A.M., & Tebaldini, S. (2008). On the Exploitation of Target Statistics for SAR Interferometry Applications. *IEEE Transactions on Geoscience and Remote Sensing, 46*, 11,3436-3443,doi:10.1109/TGRS.2008.2001756.

Hanssen, R.F. (2001). *Radar interferometry: Data interpretation and error analysis*. Springer Netherlands.

Heimlich, C., Gourmelen, N., Masson, F., Schmittbuhl, J., Kim, S., & Azzola, J. (2015). Uplift around the geothermal power plant of Landau (Germany) as observed by InSAR monitoring. *Geothermal Energy 3*,doi:https://doi.org/10.1186/s40517-014-0024-y.

Hooper, A. (2008). A multi-temporal InSAR method incorporating both persistent scatterer and small baseline approaches. *Geophysical Research Letters, 35*, 16,doi:10.1029/2008GL034654.

Hooper, A., Bekaert, D., Spaans, K., & Arikan, M. (2012). Recent advances in SAR interferometry time series analysis for measuring crustal deformation. *Tectonophysics, 514 517*,1-13,doi:https://doi.org/10.1016/j.tecto.2011.10.013.

Hooper, A., Segall, P., & Zebker, H. (2007). Persistent scatterer interferometric synthetic aperture radar for crustal deformation analysis, with application to Volcán Alcedo, Galápagos. *Journal of Geophysical Research: Solid Earth, 112*, B7,doi:10.1029/2006JB004763.

Jordan, C., Bateson, L., & Novellino, A. (2019). Environmental baseline monitoring for shale-gas development: Insights for monitoring ground motion using InSAR analysis. *Science of the total Environment, 696*,134075,doi:https://doi.org/10.1016/j.scitotenv.2019.134075.

Kampes, B. (2005). Deformation parameter estimation using permanent scatterer interferometry. PhD Thesis, Delft University of Technology, Delft, The Netherlands,

Lanari, R., Mora, O., Manunta, M., Mallorqui, J.J., Berardino, P., & Sansosti, E. (2004). A small-baseline approach for investigating deformations on full-resolution differential SAR interferograms. *IEEE Transactions on Geoscience and Remote Sensing, 42*, 7,1377-1386,doi:10.1109/TGRS.2004.828196.

Mirzaee, S., Motagh, M., Akbari, B., Wetzel, H.U., & Roessner, S. (2017). Evaluating three insar time-series methods to assess creep motion, case study: Masouleh landslide in north Iran. *ISPRS Annals of the Photogrammetry, Remote Sensing and Spatial Information Sciences, IV-1-W1*, 1,223-228,doi:10.5194/isprs-annals-IV-1-W1-223-2017.

Mora, O., Mallorqui, J.J., & Broquetas, A. (2003). Linear and nonlinear terrain deformation maps from a reduced set of interferometric SAR images. *IEEE Transactions on Geoscience and Remote Sensing, 41*, 10,2243-2253,doi:https://doi.org/10.1109/TGRS.2003.814657.

Osmanoğlu, B., Sunar, F., Wdowinski, S., & Cabral-Cano, E. (2016). Time series analysis of InSAR data: Methods and trends. *ISPRS Journal of Photogrammetry and Remote Sensing, 115*,90-102,doi:https://doi.org/10.1016/j.isprsjprs.2015.10.003.

Pepe, A., & Calo, F. (2017). A review of interferometric synthetic aperture RADAR (InSAR) multi-track approaches for the retrieval of Earth's surface displacements. *Applied Sciences, 7*, 12,1264,doi:https://doi.org/10.3390/app7121264.

Raucoules, D., Bourgine, B., de Michele, M., Le Cozannet, G., Closset, L., Bremmer, C., Veldkamp, H., Tragheim, D., Bateson, L., Crosetto, M., Agudo, M., & Engdahl, M. (2009). Validation and intercomparison of Persistent Scatterers Interferometry: PSIC4 project results. *Journal of Applied Geophysics, 68*, 3,335-347,doi:10.1016/j.jappgeo.2009.02.003.

Sadeghi, Z., Valadan Zoej, M., Hooper, A., & Lopez - Sanchez, J. (2018). A New Polarimetric Persistent Scatterer Interferometry Method Using Temporal Coherence Optimization. *IEEE Transactions on Geoscience and Remote Sensing, 56*, 11,6547-6555. ISSN 0196-2892,doi:https://doi.org/10.1109/TGRS.2018.2840423.

Schmidt, D.A., & Bürgmann, R. (2003). Time-dependent land uplift and subsidence in the Santa Clara valley, California, from a large interferometric synthetic aperture radar data set. *Journal of Geophysical Research: Solid Earth, 108*, B9,doi:10.1029/2002JB002267.

Shanker, P., Casu, F., Zebker, H.A., & Lanari, R. (2011). Comparison of Persistent Scatterers and Small Baseline Time-Series InSAR Results: A Case Study of the San Francisco Bay Area. *IEEE Geoscience and Remote Sensing Letters, 8*, 4,592-596,doi:10.1109/LGRS.2010.2095829.

Sousa, J.J., Hooper, A.J., Hanssen, R.F., Bastos, L.C., & Ruiz, A.M. (2011). Persistent Scatterer InSAR: A comparison of methodologies based on a model of temporal deformation vs. spatial correlation selection criteria. *Remote Sensing of Environment, 115*, 10,2652-2663,doi:10.1016/j.rse.2011.05.021.

Sowter, A., Bateson, L., Strange, P., Ambrose, K., & Syafiudin, M.F. (2013). DInSAR estimation of land motion using intermittent coherence with application to the South Derbyshire and Leicestershire coalfields. *Remote Sensing Letters, 4*, 10,979-987,doi:10.1080/2150704X.2013.823673.

Spaans, K., & Hooper, A. (2016). InSAR processing for volcano monitoring and other near-real time applications. *Journal of Geophysical Research: Solid Earth, 121*, 4,2947-2960,doi:https://doi.org/10.1002/2015JB012752.

Van der Kooij, M., Hughes, W., Sato, S., & Poncos, V. (2005). Coherent target monitoring at high spatial density: examples of validation results. In, *Fringe , ESA*

Werner, C., Wegmuller, U., Strozzi, T., & Wiesmann, A. (2003). Interferometric point target analysis for deformation mapping. In, *IGARSS, IEEE* (pp. 4362-4364)